Weaver, P.P.E., Schmincke, H.-U., Firth, J.V., and Duffield, W. (Eds.), 1998
Proceedings of the Ocean Drilling Program, Scientific Results, Vol. 157

19. $^{40}Ar/^{39}Ar$ AGES OF PLIOCENE–PLEISTOCENE FALLOUT TEPHRA LAYERS AND VOLCANICLASTIC DEPOSITS IN THE SEDIMENTARY APRONS OF GRAN CANARIA AND TENERIFE (SITES 953, 954, AND 956)[1]

Paul van den Bogaard[2]

ABSTRACT

Six fallout tephra layers and 16 heterolithologic volcaniclastic deposits drilled at Holes 953A, 954A, 954B, and 956A, during Leg 157 in the sedimentary aprons of Gran Canaria and Tenerife, have been dated by single crystal laser $^{40}Ar/^{39}Ar$ analysis. The fallout tephra markers range in age from 0.273 ± 0.006 Ma to 2.74 ± 0.01 Ma. Maximum sedimentation ages determined for the volcaniclastic deposits range from 0.24 ± 0.01 Ma to 2.24 ± 0.02 Ma, closely matching the nannofossil and paleomagnetic chronostratigraphies of the cores. Both tephra and volcaniclastic layers represent material from Pliocene–Pleistocene explosive eruptions of the Cañadas Caldera (Tenerife), mixed with Miocene volcanic debris only in the holes drilled north of Gran Canaria (954A and 954B). Two fallout layers (0.61 ± 0.02 Ma and 1.83 ± 0.02 Ma) and five volcaniclastic deposits reflect explosive eruptions, which took place during postulated dormant stages of the Cañadas edifice.

INTRODUCTION

Miocene to Pleistocene submarine tephra layers and volcaniclastic deposits recovered during Leg 157 (Volcanic Island Clastic Apron Project) reflect the Cenozoic submarine to subaerial volcanic activity of the Canary Island magma systems and the sedimentary evolution of the island's submarine volcaniclastic wedges. This paper presents the results of geochronological studies of upper Pliocene to Pleistocene fallout tephra layers and volcaniclastic sediments recovered at Sites 953, 954, and 956. The aim of the study is to define and date chronostratigraphic markers (ash layers) that permit the direct correlation of subaerial ocean island volcanic phases with the marine volcaniclastic record of the sedimentary apron, and to evaluate the chronostratigraphic significance of volcaniclastic deposits in the clastic aprons through single crystal $^{40}Ar/^{39}Ar$ laser dating of their volcanic mineral components.

Fallout tephra deposits, and various types of subaerial and submarine pyroclastic flow deposits and their more widespread co-genetic ash cloud deposits, are immediately derived from explosive volcanic eruptions. The time between cooling and isotopic closure of juvenile crystals in primary tephra deposits differs only insignificantly (minutes to months) from the actual time of deposition. Contaminant older crystals are rare in most fallout tephra deposits and often easily distinguished from juvenile crystal components by their mineral and chemical composition. Isotopically homogeneous (or isochronous) crystal populations, thus, make fallout tephra layers ideal chronostratigraphic markers that can be traced over long distances and different depositional environments, and whose age can be determined with high precision through K-Ar and $^{40}Ar/^{39}Ar$ dating methods.

Volcaniclastic deposits range from tephra layers that were merely remobilized and transported over short distances during or shortly after deposition with little or no erosion or admixing of foreign sediment material, to epiclastic sands, lahars, debris flows, large submarine mass flows, and turbidity currents that collect and mix lithic and biogenic sediment material from many different sources generally varying in age and composition. The age of deposition of volcaniclastic sediments poses important constraints on the temporal evolution of the clastic aprons, the rates and processes of mass transfer from the ocean islands into the surrounding sedimentary basins, and erosional intervals and major tectonic events on the ocean islands themselves (Schmincke and Bogaard, 1990). Contrary to primary tephra layers, however, volcaniclastic sediments are notoriously difficult to date directly.

While volcaniclastic deposits form in the sedimentary apron of volcanic ocean islands, explosive eruptions from active magma systems provide a more or less continuous supply of juvenile potassium-rich crystals, whose argon isotope composition records the age of individual eruptions. Moreover, the eruptions themselves and the rapid accumulation of tephra material on the slopes of volcanic islands, often immediately trigger the generation of (and become incorporated in) subaerial and submarine volcaniclastic deposits. Thus, the youngest volcanic crystal (or crystals) in a volcaniclastic sediments can give a reasonable maximum age estimate of the formation of the deposits, in some cases even the accurate age.

If crystals of different age and provenance are found in volcaniclastic sediments (and the mineral separate resulting from a sediment sample), which can not be clearly distinguished by means of their macro- or microscopical mineral characteristics, it thus becomes difficult to impossible to derive geologically meaningful age estimates through analytical methods that require multiple-grain mineral separates, such as K-Ar dating. $^{40}Ar/^{39}Ar$ step-heating analysis can qualitatively discriminate different age populations within mineral separates if the crystal populations differ significantly in their closure temperature and/or temperature-dependent degassing behavior. The latter, however, is generally not true for crystals of the same mineral species that are similar in origin and chemical composition, and derived from the same long-lived magma systems through a series of individual eruptions over a long period of time (up to millions of years). The problem can only be tackled by single-grain analytical methods such as laser $^{40}Ar/^{39}Ar$ dating.

SETTING AND STATISTICS OF SITES 953–956

During Leg 157, four sites (953 through 956) were drilled in the clastic sedimentary aprons of Gran Canaria and Tenerife, located 34 km (Site 954) to 68 km northeast (Site 953), 56 km southeast (Site 955), and ~50 km southwest of Gran Canaria (Site 956) at water depths ranging from 2854.1 m (Site 955) to 3577.8 m (Site 953; Fig. 1). The complete statistics of each hole are given in Table 1.

[1]Weaver, P.P.E., Schmincke, H.-U., Firth, J.V., and Duffield, W. (Eds.), 1998. *Proc. ODP, Sci. Results*, 157: College Station, TX (Ocean Drilling Program).

[2]GEOMAR Forschungszentrum, Wischhofstrasse 1-3, D-24148 Kiel, Federal Republic of Germany. pbogaard@geomar.de

The tephra deposits studied here are exclusively from the uppermost, upper Pliocene to Pleistocene lithostratigraphic Unit I of Cores 953A, 954A, 954B, and 956A. At Site 953, Unit I (0–197 meters below seafloor [mbsf]) predominantly comprises pelagic clayey nannofossil ooze and graded nannofossil silt, with interbeds of crystal-, foraminifer-, or lithic-rich sands and silt, volcaniclastic sands rich in neritic fossils, and minor thin fallout tephra layers. At Site 954, Unit I (0–158 mbsf) consists chiefly of clayey nannofossil ooze, graded clayey nannofossil mixed sediment, and calcareous lithic sands, and again minor interbeds of crystal lithic sand, pumice sand, vitric ash layers, and coarse volcaniclastic sands rich in neritic biogenic material. At Site 956, Unit I (0–158 mbsf) consists mostly of nannofossil mixed sediments with foraminifers and abundant interbedded thick, coarse, pumice-rich debris flows and fallout ash layers, and is characterized by abundant sediment slumps. The fallout ash layers and the pumiceous debris flows at Site 956 are tentatively attributed to volcanic eruptions from Tenerife. The coarse neritic sands at Sites 953 and 954 are interpreted to represent beach sands remobilized in turbidity currents (Schmincke, Weaver, Firth, et al., 1995).

ANALYTICAL METHODS

All ash layers, ash-bearing sediments, and volcaniclastic deposits studied here have been identified by the Shipboard Scientific Party (Schmincke, Weaver, Firth, et al., 1995) and were sampled on the *JOIDES Resolution.* According to shipboard core descriptions and laboratory assessments, the samples comprised six distinctive, well-sorted, homogeneous fallout ash layers, and 16 volcaniclastic deposits ranging from well-sorted pumice-, lithic-, or crystal-bearing epiclastic sands and silts and poorly sorted, heterolithologic lapillistone breccia beds, and debris flow deposits.

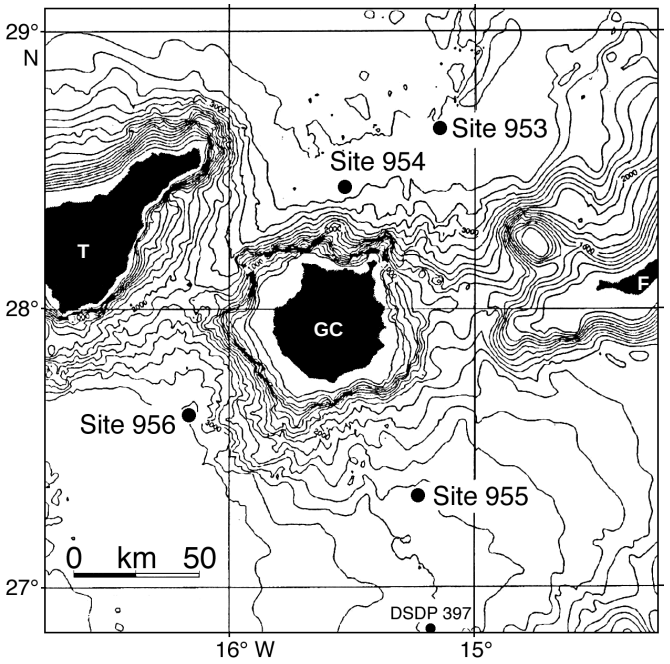

Figure 1. Location of Sites 953, 954, 955, and 956 in the Canaries archipelago.

Samples were washed and wet sieved, and feldspar crystals were separated from the 0.25- to 0.5-mm and 0.5- to 1-mm grain-size fractions using a vacuum tweezer under a binocular microscope. Separated crystals were then etched in hydrofluoric acid and cleaned with an ultrasonic disintegrator. The crystals were irradiated in aluminum sample holders in the 5 MW reactor at the GKSS Research Center (Geesthacht, FRG) for 72 hr at an average fast neutron flux of 2.1×10^{12} N/cm^{2}xs, shielded by 0.5 mm Cd foil. The neutron flux was monitored using TCR sanidine (27.92 Ma; Dalrymple and Duffield, 1988; Duffield and Dalrymple, 1990). Vertical variations in J-value were quantified by a cosine function fit (Table 2).

All age determinations were conducted by $^{40}Ar/^{39}Ar$ laser dating of single feldspar crystals, applying a 25 W Spectra Physics Argon Ion laser, and MAP 216 series noble gas mass spectrometer. Raw mass spectrometer peaks were corrected for mass discrimination and system blanks. Interfering neutron reactions were quantified using pure K_2SO_4 crystals and optical grade CaF_2 crystals that were irradiated together with the feldspar samples (this irradiation: $[^{36}Ar/^{39}Ar]_{Ca}$ = 0.465 ± 0.001, $[^{37}Ar/^{39}Ar]_{Ca}$ = 977 ± 2, $[^{40}Ar/^{39}Ar]_{K}$ = 0.002 ± 0.001]). The single crystal dating results are discussed by means of isotope correlation (York, 1969) and their mean apparent ages, weighted by the inverse variance. Analytical uncertainties are given as 1 sigma errors. $^{40}Ar/^{39}Ar$ dating results are summarized in Table 2. Single crystal data are listed in Table 3.

AGE DETERMINATIONS

Fallout Ash Layers

Sample 157-953A-2H-5, 147–150 cm, represents the bottom part of a ~4-cm-thick, homogeneous, gray, coarse-grained, well-sorted, pumice- and feldspar-rich fallout ash layer. A total of 22 feldspar crystals, 0.057–1.005 mg in mass, were analyzed and yielded apparent ages ranging from 0.20 ± 0.04 Ma to 0.35 ± 0.03 Ma (Table 3). Isotope correlation returns an isochron age of 0.28 ± 0.01 Ma with an initial $^{40}Ar/^{36}Ar$ ratio of 341 ± 73 (mean square weighted deviates [MSWD] = 3.13), which is not significantly different from an atmospheric initial $^{40}Ar/^{36}Ar$ ratio of 295.5 (Fig. 2). The weighted mean apparent age of the entire population is 0.284 ± 0.005 Ma (MSWD = 3.18). The relatively high scatter and MSWD indicates that slightly older xenocrysts may have been incorporated by the magma prior to eruption or were added to the tephra during the eruption. Excluding six crystals with apparent ages >0.3 Ma from the weighted average reduces the MSWD to an acceptable level (2.48), and yields a mean apparent age of 0.273 ± 0.006 Ma, which is interpreted here as the eruption age of tephra Sample 157-953A-2H-5, 147–150 cm.

Sample 157-953A-5H-1, 56–57 cm, represents a dark green, fine-grained, well-sorted, vitric fallout ash layer. Eight anorthoclase feld-

Table 1. Statistics of Leg 157 sites discussed in this paper.

	Site 953	Site 954		Site 956
Hole	953A	954A	954B	956A
Latitude	28°39.023′N	28°26.197′N	28°26.191′N	27°36.905′N
Longitude	15°8.681′W	15°31.928′W	15°31.921′W	16°9.797′W
Water depth (m)	3577.8	3485.2	3485.2	3441.9
Total penetration (m)	192.6	83.8	446.0	161.6
Total length of cored section (m)	192.6	83.8	365.8	161.6
Core recovery (%)	102.6	96	45.3	99.3
Depth (mbsf)	192.6	83.8	365.8	161.6
Earliest age	Late Pliocene	Pleistocene	Middle Miocene	Early Pliocene

Note: Data taken from Schmincke, Weaver, Firth, et al. (1995).

Table 2. Feldspar crystal populations from Pliocene–Pleistocene fallout tephra layers and volcaniclastic sediments, Holes 953A, 954A, 954B, and 956B.

Core, section, interval (cm)		Depth (mbsf)	N	Mean age (Ma) ± 1 sigma	MSWD	N used	Isochron age (Ma) ± 1 sigma	Initial $^{40}Ar/^{36}Ar$ ± 1 sigma	MSWD	N used	J ± 1 sigma	Lab number
157-953A-												
2H-4, 77-79	V	12.87	4	0.246 ± 0.009	1.01	4	n.a.				9.085E-04 ± 9.5E-07	8114
2H-5, 147-150	T	15.08	22	0.284 ± 0.005	3.18	22	0.28 ± 0.01	341± 73	3.13	22		8002/8115
											8.880E-04 ± 1.2E-06	8002
											9.085E-04 ± 9.5E-07	8115
5H-1, 56-57	T	36.66	9	0.61 ± 0.02	0.62	8	0.42 ± 0.78	621 ± 1269	0.58	8	9.085E-04 ± 9.5E-07	8116
14H-1, 83-84	T	122.43	4	1.83 ± 0.02	1.68	4	1.40 ± 3.60	1270 ± 8800	1.68	4	9.085E-04 ± 9.5E-07	8118
157-954A-												
4H-6, 58-64	V	28.08	8	2.13 ± 0.07	n.a.	1	4.60 ± 3.80	11444 ± 5413	2	8	8.946E-04 ± 1.0E-06	8036
7H-5, 94-100	V	55.44	11	0.89 ± 0.02	0.13	5	n.a.				8.946E-04 ± 1.0E-06	8037
8H-3, 81-86	V	61.81	11	0.86 ± 0.01	n.a.	1	n.a.				8.946E-04 ± 1.0E-06	8039
9H-4, 26-31	V	72.26	11	1.15 ± 0.04	2.22	6	n.a.				8.946E-04 ± 1.0E-06	8042
157-954B-												
1R-1, 64-72	V	80.84	5	1.46 ± 0.04	0.4	4	1.43 ± 0.07	325 ± 55	0.22	4	9.085E-04 ± 9.5E-07	8043
4R-2, 37-51	T	111.61	21	2.37 ± 0.02	1.86	21	2.47 ± 0.03	151 ± 44	1.32	21		8045/8046
											8.946E-04 ± 1.0E-06	8045
											9.124E-04 ± 1.0E-06	8046
5R-3, 71-73	T	123.01	11	2.74 ± 0.01	0.63	11	2.78 ± 0.02	202 ± 58	0.52	11	9.085E-04 ± 9.5E-07	8122
157-956B-												
3H-2, 81-87	V	17.91	11	0.24 ± 0.01	n.a.	1	n.a.				8.946E-04 ± 1.0E-06	8077
6H-1, 5-12	V	44.15	11	1.68 ± 0.02	0.78	11	1.71 ± 0.04	276 ± 32	0.82	11	9.085E-04 ± 9.5E-07	8078
6H-2, 120-122	V	46.80	2	1.67 ± 0.02	n.a.	2	n.a.				9.085E-04 ± 9.5E-07	8124
6H-2, 124-126	V	46.84	4	1.70 ± 0.01	0.39	4	1.71 ± 0.02	259 ± 109	0.54	4	9.085E-04 ± 9.5E-07	8125
7H-5, 107-109	V	60.67	13	2.00 ± 0.05	2.89	12	1.98 ± 0.07	437 ± 38	0.38	12	9.085E-04 ± 9.5E-07	8126
7H-6, 108-122	V	62.18	11	2.04 ± 0.02	2.61	9	2.06 ± 0.06	289 ± 26	3.04	9	8.946E-04 ± 1.0E-06	8079
8H-3, 14-19	V	66.24	11	2.04 ± 0.02	1.99	10	2.03 ± 0.03	303 ± 8	1.83	10	8.946E-04 ± 1.0E-06	8080
8H-6, 20-26	V	70.80	6	2.13 ± 0.02	1.04	6	2.16 ± 0.04	256 ± 204	1.31	6	9.124E-04 ± 1.0E-06	8081
9H-1, 33-34	V	72.93	7	2.24 ± 0.02	1.41	7	n.a.				9.085E-04 ± 9.5E-07	8128
9H-2, 36-42	V	74.46	10	2.19 ± 0.02	1.22	7	2.10 ± 0.06	576 ± 136	1.61	10	9.124E-04 ± 1.0E-06	8083
11H-2, 68-70	T	93.78	13	2.47 ± 0.02	1.06	13	2.10 ± 0.90	965 ± 1550	0.84	13	9.085E-04 ± 9.5E-07	8130

Notes: Samples 80028115 and 80458046 were irradiated in two different batches. N = number of crystals analyzed, N used = number of crystals used to calculate mean apparent age and isochron age, MSWD = mean square weighted deviates, J = neutron flux correction factor, V= volcaniclastic deposit, T = fallout tephra, and n.a. = not applicable.

spars were separated and analyzed from this sample. They ranged in mass from 0.08 to 0.15 mg and gave apparent ages from 0.5 ± 0.1 to 0.72 ± 0.07 Ma (Table 3). Although their isochron age (0.4 ± 0.8 Ma) and initial $^{40}Ar/^{36}Ar$ ratio (620 ± 1270) are poorly defined, all single crystal analyses are compatible with a weighted mean apparent age of 0.61 ± 0.02 Ma (MSWD = 0.62).

Sample 157-953A-14H-1, 83–84 cm, is a thin, moderately sorted fallout ash layer dispersed in nannofossil clay. Only four anorthoclase feldspar crystals (0.18–0.30 mg) were recovered from this sample, yielding apparent ages from 1.80 ± 0.03 to 1.88 ± 0.03 Ma. Again, isochron age and initial $^{40}Ar/^{36}Ar$ ratio (1300 ± 8800) are poorly constrained (Fig. 2), but the mean apparent age is fine (1.83 ± 0.02 Ma; MSWD = 1.68) and interpreted to reflect the eruption age of tephra Sample 157-953A-14H-1, 83–84 cm.

Samples 157-954B-4R-2, 37–43 cm, and 45–51 cm, are from a single, ~14-cm-thick, well-sorted, crystal-rich, vitric, pumice-bearing fallout ash layer, here referred to as tephra Sample 157-954B-4R-2, 37–51 cm. Twenty-one anorthoclase crystals (0.07–0.18 mg) from this sample range in apparent age from 2.24 ± 0.05 to 2.50 ± 0.09 Ma (Table 3). With atmospheric ^{40}Ar percentages ranging from 1% to 14%, their argon isotope compositions form a scattered cluster near the $^{39}Ar/^{40}Ar$ axis in the isotope correlation diagram (Fig. 2), which does not permit reliable estimates of the initial $^{40}Ar/^{36}Ar$ ratio of the population. Therefore, the mean apparent age (2.37 ± 0.02 Ma; MSWD = 1.86) is interpreted to give the best estimate of the eruption age of tephra Sample 157-954B-4R-2, 37–51 cm.

Sample 157-954B-5R-3, 71–73 cm, represents a coarse-grained, distinct, pumiceous fallout ash layer. Eleven anorthoclase crystals (0.08–0.27 mg) were analyzed, their single grain ages ranging from 2.67 ± 0.06 to 2.80 ± 0.04 Ma. Isotope correlation gives an isochron age of 2.78 ± 0.02 Ma (MSWD = 0.52), but another poor estimate of the initial $^{40}Ar/^{36}Ar$ ratio (202 ± 58). The eruption age of tephra Sample 157-954B-5R-3, 71–73 cm, is therefore determined as 2.74 ± 0.01 Ma (mean apparent age: MSWD = 0.63).

Sample 157-956A-11H-2, 68–70 cm, is the only distinct fallout ash layer from Site 956 analyzed here. It is well-sorted, vitric, and crystal-rich. Thirteen anorthoclase crystals (0.074–0.18 mg each) were dated with apparent ages from 2.40 ± 0.05 to 2.59 ± 0.11 Ma. Isotope correlation returns a poor estimate of the initial $^{40}Ar/^{36}Ar$ ratio (965 ± 1550) and, thus, an unreliable isochron age of 2.1 ± 0.9 Ma. The weighted average of the apparent ages indicates a homogeneous crystal population (MSWD = 1.06) and an eruption age of 2.47 ± 0.02 Ma.

Volcaniclastic Deposits

Sample 157-953A-2H-4, 77–79 cm, is a gray, crystal- and lithic-rich volcaniclastic sand deposit with abundant calcareous fossil shells. Only four anorthoclase crystals (0.056–0.361 mg) were recovered from this unit and yielded apparent ages from 0.17 ± 0.05 to 0.26 ± 0.02 Ma (Fig. 3), and a mean apparent age of 0.246 ± 0.009 Ma (MSWD = 1.01).

Sample 157-954A-4H-6, 58–64 cm, consists of calcareous volcaniclastic sand rich in pumice fragments, glass shards, and crystals. Eight anorthoclase feldspar crystals (0.043–0.170 mg) were analyzed, one of which yielded an apparent age of 2.13 ± 0.07 Ma. The other seven crystals show apparent ages ranging from 10.0 to 11.7 Ma (Fig. 3).

Sample 157-954A-7H-5, 94–100 cm, is from a coarse-grained, calcareous, volcaniclastic sand deposit with abundant feldspar crystals and fragments of basalt, sideromelane, and phonolite rocks. Its feldspar crystals (0.10–0.20 mg) fall into three distinct groups. Group one is composed of five anorthoclase and plagioclase crystals with apparent ages ~0.9 Ma. This population defines an isochron with an age of 0.91 ± 0.02 Ma, and an initial $^{40}Ar/^{36}Ar$ ratio of 277 ± 30 (MSWD = 0.14; Fig. 3). The second group contains two plagioclase crystals with apparent ages ~1.4 Ma. The third group is composed of four crystals with apparent ages ranging from 10.05 ± 0.04 Ma to 13.80 ± 0.03 Ma. The mean apparent age of population 1 (0.89 ± 0.02 Ma; MSWD = 0.13) constrains the maximum age of this volcaniclastic layer.

Sample 157-954A-8H-3, 81–86 cm, is from the base of a 16-cm-thick, crystal- and lithic-rich volcaniclastic sand deposit. The deposit shows an age spectrum similar to Sample 157-954A-7H-5, 94–100

Table 3. Single crystal $^{40}Ar/^{39}Ar$ ages.

Core, section, interval (cm)	Lab number	Age (yr)	1σ (yr)	$^{40}Ar^*/^{39}Ar_K$	% $^{40}Ar_{atm}$	Ca/K	Mass (mg)	Volume ^{39}Ar (ccSTP/mg)
157-953A-	8114-1	1.68E+05	5.3E+04	1.0261E-01	5.07E+01	4.26E-02	0.056	3.37E-10
2H-4, 77-79	8114-2	2.22E+05	3.1E+04	1.3518E-01	4.17E+01	1.02E-01	0.249	2.11E-10
	8114-3	2.55E+05	2.0E+04	1.5531E-01	2.94E+01	1.30E-01	0.207	2.82E-10
	8114-4	2.50E+05	1.1E+04	1.5231E-01	3.44E+01	1.04E-01	0.361	3.10E-10
2H-5, 147-150	8002-1	3.16E+05	1.6E+05	1.9712E-01	7.86E+01	9.44E+00	0.227	1.72E-11
	8002-2	3.09E+05	3.6E+04	1.9259E-01	3.23E+01	4.26E-01	0.202	1.82E-10
	8002-3	2.60E+05	1.2E+04	1.6229E-01	1.92E+01	6.27E-02	0.321	3.16E-10
	8002-4	2.77E+05	1.3E+04	1.7289E-01	2.00E+01	8.05E-02	0.262	2.93E-10
	8002-5	2.51E+05	1.9E+04	1.5678E-01	2.71E+01	7.21E-02	0.212	2.86E-10
	8002-6	2.38E+05	1.3E+04	1.4865E-01	2.59E+01	3.33E-02	0.336	3.41E-10
	8002-7	2.91E+05	2.0E+04	1.8135E-01	2.93E+01	1.68E-01	0.286	2.57E-10
	8002-8	2.81E+05	2.1E+04	1.7563E-01	2.80E+01	2.52E-01	0.249	2.24E-10
	8002-9	2.89E+05	5.1E+03	1.8055E-01	1.20E+01	1.03E-01	0.968	2.40E-10
	8002-10	3.05E+05	6.0E+03	1.9054E-01	1.87E+01	2.03E-01	1.005	2.35E-10
	8002-11	2.92E+05	8.2E+04	1.8246E-01	5.75E+01	5.76E-01	0.057	1.65E-10
	8002-12	2.68E+05	3.1E+04	1.6735E-01	2.48E+01	7.06E-02	0.131	2.56E-10
	8002-13	2.39E+05	3.2E+04	1.4940E-01	4.10E+01	8.13E-02	0.085	2.95E-10
	8115-14	2.59E+05	2.9E+04	1.5802E-01	3.31E+01	1.05E-01	0.181	2.83E-10
	8115-15	3.20E+05	6.4E+04	1.9502E-01	1.73E+01	1.92E-02	0.103	3.72E-10
	8115-16	3.46E+05	2.7E+04	2.1112E-01	1.67E+01	2.10E-02	0.142	3.84E-10
	8115-17	3.27E+05	3.1E+04	1.9946E-01	5.99E+00	1.04E-01	0.187	3.23E-10
	8115-18	2.48E+05	2.2E+04	1.5146E-01	3.53E+01	5.64E-02	0.175	3.44E-10
	8115-19	2.46E+05	2.5E+04	1.5023E-01	2.20E+01	2.32E-02	0.176	3.25E-10
	8115-20	2.03E+05	2.7E+04	1.2384E-01	4.34E+01	6.81E-02	0.141	2.84E-10
	8115-21	2.41E+05	3.0E+04	1.4677E-01	3.15E+01	3.01E-02	0.160	3.28E-10
	8115-22	2.00E+05	3.6E+04	1.2183E-01	4.62E+01	2.61E-02	0.124	3.49E-10
5H-1, 56-57	8116-1	6.03E+05	3.0E+04	3.6795E-01	1.93E+01	5.78E-02	0.146	2.42E-10
	8116-2	6.38E+05	7.5E+04	3.8943E-01	2.69E+01	4.45E-02	0.079	2.16E-10
	8116-3	4.97E+05	1.3E+05	3.0310E-01	3.60E+01	4.15E-02	0.090	1.77E-10
	8116-4	6.25E+05	6.0E+04	3.8164E-01	2.55E+01	7.10E-02	0.118	2.13E-10
	8116-5	6.22E+05	7.2E+04	3.7966E-01	1.81E+01	5.93E-02	0.120	2.35E-10
	8116-6	5.82E+05	4.0E+04	3.5490E-01	2.60E+01	4.42E-02	0.150	2.53E-10
	8116-7	6.10E+05	3.5E+04	3.7252E-01	2.53E+01	5.33E-02	0.142	2.51E-10
	8116-8	7.24E+05	6.8E+04	4.4191E-01	1.09E+01	4.94E-02	0.091	2.41E-10
14H-1, 83-84	8118-1	1.87E+06	4.8E+04	1.1444E+00	2.68E+00	1.29E-01	0.184	1.60E-10
	8118-2	1.82E+06	1.6E+04	1.1120E+00	5.79E+00	5.23E-02	0.221	2.16E-10
	8118-3	1.80E+06	2.6E+04	1.0990E+00	8.29E+00	2.48E-01	0.299	1.38E-10
	8118-4	1.88E+06	3.2E+04	1.1481E+00	5.79E+00	1.17E-01	0.256	1.67E-10
157-954A-	8036-1	1.02E+07	6.0E+04	6.3393E+00	2.02E+00	8.89E-02	0.063	2.80E-10
4H-6, 58-64	8036-2	1.17E+07	2.1E+06	7.2890E+00	2.01E-01	4.85E-02	0.050	3.02E-10
	8036-3	1.07E+07	1.3E+05	6.6460E+00	8.76E-01	4.18E-02	0.043	2.78E-10
	8036-4	1.01E+07	1.0E+05	6.2967E+00	7.60E-01	7.16E-02	0.054	2.68E-10
	8036-5	2.13E+06	7.0E+04	1.3191E+00	3.21E+00	5.04E-02	0.065	2.81E-10
	8036-6	1.06E+07	1.2E+05	6.5579E+00	3.91E+00	5.27E-02	0.041	2.76E-10
	8036-7	1.00E+07	1.2E+05	6.2124E+00	1.26E+00	8.41E-02	0.152	2.45E-10
	8036-8	1.05E+07	1.3E+05	6.5349E+00	1.86E+00	6.48E-02	0.170	1.85E-10
7H-5, 94-100	8037-1	1.36E+07	4.1E+04	8.4702E+00	1.32E+00	2.91E-02	0.134	1.89E-10
	8037-2	1.38E+06	3.0E+04	8.5549E-01	3.16E+01	1.77E-02	0.196	2.32E-10
	8037-3	8.75E+05	3.1E+04	5.4246E-01	2.13E+01	6.89E-02	0.195	2.33E-10
	8037-4	1.46E+06	8.6E+04	9.0229E-01	3.11E+01	9.47E-01	0.172	8.59E-11
	8037-5	9.01E+05	2.3E+04	5.5867E-01	1.68E+01	8.76E-02	0.151	2.16E-10
	8037-6	9.50E+05	5.3E+05	5.8895E-01	7.03E+01	2.30E+01	0.182	1.69E-11
	8037-7	1.01E+06	5.1E+05	6.2720E-01	6.37E+01	1.75E+01	0.135	1.99E-11
	8037-8	1.00E+07	4.1E+04	6.2425E+00	2.68E+00	3.79E-02	0.158	2.22E-10
	8037-9	1.36E+07	4.8E+04	8.4382E+00	1.95E+00	6.00E-03	0.202	2.05E-10
	8037-10	8.83E+05	4.5E+05	5.4738E-01	7.90E+01	3.00E+01	0.159	1.36E-11
	8037-11	1.32E+07	1.1E+05	8.2239E+00	2.53E+00	2.19E-02	0.104	1.54E-10
8H-3, 81-86	8039-1	1.83E+06	2.8E+04	1.1372E+00	3.30E+00	1.02E-01	0.252	1.79E-10
	8039-2	1.35E+07	4.4E+04	8.3915E+00	2.88E+00	2.80E-02	1.406	1.83E-10
	8039-3	9.23E+05	5.0E+03	5.7216E-01	4.00E+00	4.68E-02	1.195	2.58E-10
	8039-4	9.43E+05	1.3E+04	5.8427E-01	5.92E+00	7.78E-02	0.500	2.42E-10
	8039-5	9.23E+05	9.3E+03	5.7175E-01	4.35E+00	5.83E-02	0.713	2.41E-10
	8039-6	1.59E+06	1.9E+05	9.8859E-01	4.17E+01	2.05E+01	0.523	1.56E-11
	8039-7	9.79E+05	1.0E+04	6.0651E-01	7.21E+00	1.26E-01	0.804	2.21E-10
	8039-8	1.30E+07	4.2E+04	8.1026E+00	5.77E+00	7.47E-02	0.977	1.92E-10
	8039-9	9.43E+05	6.4E+03	5.8426E-01	6.21E+00	8.62E-02	1.004	2.22E-10
	8039-10	9.17E+05	5.4E+03	5.6835E-01	6.41E+00	4.20E-02	0.923	2.52E-10
	8039-11	8.59E+05	1.1E+04	5.3211E-01	1.16E+01	4.08E-02	0.379	2.51E-10
9H-4, 26-31	8042-1	1.14E+06	2.9E+04	7.0445E-01	1.07E+01	1.22E-01	0.150	2.38E-10
	8042-2	9.96E+06	3.3E+04	6.1870E+00	5.43E-01	7.04E-02	0.380	2.17E-10
	8042-3	1.29E+07	4.2E+04	8.0445E+00	6.34E-01	2.49E-02	0.216	2.25E-10
	8042-4	1.84E+06	4.5E+04	1.1414E+00	2.25E+00	1.02E-01	0.217	1.67E-10
	8042-5	1.64E+06	1.7E+05	1.0141E+00	1.79E+01	8.25E+00	0.323	3.06E-11
	8042-6	1.24E+06	2.9E+05	7.7151E-01	3.01E+01	8.74E+00	0.166	2.71E-11
	8042-7	2.76E+06	3.7E+05	1.7089E+00	1.22E+00	1.85E+01	0.142	1.52E-11
	8042-8	1.81E+06	1.1E+05	1.1198E+00	1.19E+01	6.68E-01	0.100	9.46E-11
	8042-9	1.27E+06	1.8E+05	7.8817E-01	3.29E+01	1.01E+01	0.287	2.41E-11
	8042-10	1.45E+06	4.8E+05	8.9942E-01	6.86E+01	1.49E+01	0.108	1.84E-11
	8042-11	6.38E+05	4.3E+05	3.9527E-01	7.15E+01	1.92E+01	0.114	1.57E-11
157-954B-	8043-1	2.04E+06	5.6E+05	1.2452E+00	5.20E+01	1.77E+01	0.148	1.88E-11
1R-1, 64-72	8043-2	1.38E+07	5.0E+05	8.4228E+00	2.15E+00	3.89E-01	0.296	8.57E-11
	8043-3	1.47E+06	6.6E+04	8.9604E-01	2.09E+01	3.72E-02	0.444	1.61E-10
	8043-4	1.44E+06	7.0E+04	8.7846E-01	2.33E+01	6.53E-02	0.281	1.55E-10
	8043-5	1.46E+06	5.8E+04	8.9221E-01	1.05E+01	4.59E-02	1.294	1.61E-10

Table 3 (continued).

Core, section, interval (cm)	Lab number	Age (yr)	1σ (yr)	$^{40}Ar^*/^{39}Ar_K$	% $^{40}Ar_{atm}$	Ca/K	Mass (mg)	Volume ^{39}Ar (ccSTP/mg)
4R-2, 37-51	8045-1	2.33E+06	5.8E+04	1.4475E+00	7.40E+00	6.30E-02	0.092	2.49E-10
	8045-2	2.42E+06	4.1E+04	1.4993E+00	3.05E+00	9.04E-02	0.172	2.04E-10
	8045-3	2.49E+06	6.8E+04	1.5436E+00	1.35E+00	5.81E-02	0.109	2.15E-10
	8045-4	2.45E+06	5.7E+04	1.5199E+00	3.63E+00	6.42E-02	0.113	2.34E-10
	8045-5	2.48E+06	5.7E+04	1.5398E+00	2.53E+00	7.25E-02	0.117	2.22E-10
	8045-6	2.50E+06	9.0E+04	1.5521E+00	1.84E+00	7.12E-02	0.074	2.09E-10
	8045-7	2.38E+06	5.8E+04	1.4747E+00	4.87E+00	5.16E-02	0.111	2.25E-10
	8045-8	2.39E+06	4.1E+04	1.4838E+00	4.41E+00	7.04E-02	0.180	2.15E-10
	8045-9	2.33E+06	4.9E+04	1.4427E+00	7.64E+00	4.83E-02	0.116	2.29E-10
	8045-10	2.34E+06	7.8E+04	1.4483E+00	7.91E+00	8.12E-02	0.097	2.18E-10
	8045-11	2.37E+06	9.2E+04	1.4682E+00	9.99E+00	6.41E-02	0.073	2.13E-10
	8046-1	2.51E+06	7.6E+04	1.5247E+00	1.12E+00	7.78E-02	0.075	2.22E-10
	8046-2	2.42E+06	5.7E+04	1.4726E+00	6.88E+00	9.71E-02	0.084	2.42E-10
	8046-3	2.46E+06	5.9E+04	1.4984E+00	6.52E+00	1.04E-01	0.108	2.09E-10
	8046-4	2.31E+06	6.5E+04	1.4061E+00	8.97E+00	1.13E-01	0.102	2.09E-10
	8046-5	2.38E+06	3.9E+04	1.4452E+00	7.08E+00	1.25E-01	0.148	2.13E-10
	8046-6	2.36E+06	4.2E+04	1.4319E+00	7.26E+00	1.35E-01	0.135	2.09E-10
	8046-7	2.39E+06	3.3E+04	1.4533E+00	5.68E+00	1.06E-01	0.130	2.50E-10
	8046-8	2.30E+06	3.5E+04	1.3956E+00	1.21E+01	1.70E-01	0.086	2.41E-10
	8046-9	2.32E+06	4.1E+04	1.4085E+00	1.39E+01	1.17E-01	0.106	2.50E-10
	8046-10	2.24E+06	4.5E+04	1.3591E+00	1.42E+01	2.45E-01	0.107	1.98E-10
5R-3, 71-73	8122-1	2.80E+06	4.2E+04	1.7093E+00	4.09E-02	8.47E-02	0.102	2.74E-10
	8122-2	2.72E+06	5.5E+04	1.6588E+00	7.32E+00	2.36E-01	0.076	2.07E-10
	8122-3	2.69E+06	4.7E+04	1.6428E+00	4.87E+00	1.69E-01	0.085	2.57E-10
	8122-4	2.73E+06	2.8E+04	1.6689E+00	5.16E+00	1.54E-01	0.203	2.23E-10
	8122-5	2.73E+06	3.3E+04	1.6671E+00	3.99E+00	1.20E-01	0.171	2.40E-10
	8122-6	2.73E+06	2.8E+04	1.6656E+00	4.25E+00	1.60E-01	0.269	2.16E-10
	8122-7	2.67E+06	6.2E+04	1.6327E+00	5.82E+00	2.56E-01	0.171	1.68E-10
	8122-8	2.74E+06	3.9E+04	1.6732E+00	4.84E+00	1.22E-01	0.205	2.34E-10
	8122-9	2.74E+06	6.2E+04	1.6706E+00	6.79E+00	3.50E-01	0.195	1.68E-10
	8122-10	2.70E+06	6.6E+04	1.6464E+00	5.61E+00	2.11E-01	0.116	2.27E-10
	8122-11	2.76E+06	1.7E+04	1.6842E+00	5.33E+00	1.56E-01	0.209	2.50E-10
157-956A-	8077-1	7.23E+05	3.2E+04	4.4784E-01	6.57E+00	5.28E-02	0.108	2.62E-10
3H-2, 81-87	8077-2	5.44E+05	3.1E+04	3.3686E-01	5.32E+01	9.72E-02	0.241	2.47E-10
	8077-3	3.06E+05	4.3E+03	1.8965E-01	1.72E+01	3.35E-01	2.408	1.95E-10
	8077-4	3.91E+05	1.2E+04	2.4215E-01	1.76E+01	1.02E-01	0.483	2.50E-10
	8077-5	7.33E+05	1.1E+04	4.5422E-01	2.48E+00	4.83E-02	0.592	2.40E-10
	8077-6	3.64E+05	5.5E+03	2.2564E-01	6.86E+00	2.39E-01	0.082	2.26E-10
	8077-7	2.44E+05	5.7E+03	1.5136E-01	1.12E+01	7.57E-02	0.777	2.59E-10
	8077-8	6.87E+05	5.5E+04	4.2553E-01	3.36E+01	1.12E-01	0.652	2.23E-10
	8077-9	6.76E+05	3.3E+04	4.1888E-01	1.53E+01	4.44E-02	0.168	2.61E-10
	8077-10	7.25E+05	2.4E+04	4.4915E-01	1.01E+01	4.62E-02	0.232	2.37E-10
	8077-11	7.03E+05	4.4E+04	4.3560E-01	2.37E+01	2.32E-01	0.222	1.31E-10
6H-1, 5-12	8078-1	1.64E+06	6.0E+04	9.9972E-01	9.54E+00	4.95E-01	0.163	1.21E-10
	8078-2	1.75E+06	7.4E+04	1.0706E+00	7.89E+00	9.81E-02	0.389	1.68E-10
	8078-3	1.73E+06	9.5E+04	1.0572E+00	2.48E+01	4.97E-01	0.300	1.05E-10
	8078-4	1.72E+06	7.8E+04	1.0515E+00	1.71E+01	2.05E-01	0.398	1.24E-10
	8078-5	1.42E+06	1.5E+05	8.6727E-01	4.70E+01	3.92E-01	0.101	1.24E-10
	8078-6	1.66E+06	1.1E+05	1.0147E+00	3.55E+01	1.50E-01	0.110	1.45E-10
	8078-7	1.64E+06	6.9E+04	1.0036E+00	5.78E+00	5.64E-02	0.308	2.25E-10
	8078-8	1.70E+06	9.0E+04	1.0377E+00	1.97E+01	1.13E-01	0.175	1.56E-10
	8078-9	1.76E+06	8.6E+04	1.0718E+00	1.48E+01	1.07E-01	0.271	1.41E-10
	8078-10	1.60E+06	7.1E+04	9.7966E-01	1.67E+01	6.35E-02	0.173	2.49E-10
	8078-11	1.74E+06	7.5E+04	1.0608E+00	1.44E+01	9.25E-02	0.387	1.60E-10
6H-2, 120-122	8124-1	1.75E+06	3.2E+04	1.0690E+00	5.78E-01	4.00E-02	0.117	2.72E-10
	8124-2	1.67E+06	6.7E+03	1.0193E+00	3.21E+00	4.75E-02	0.621	2.48E-10
6H-2, 124-126	8125-1	1.68E+06	4.3E+04	1.0262E+00	8.97E+00	5.43E-02	0.134	2.39E-10
	8125-2	1.70E+06	2.0E+04	1.0368E+00	3.22E+00	5.06E-02	0.167	2.60E-10
	8125-3	1.71E+06	1.5E+04	1.0418E+00	1.64E+00	4.24E-02	0.224	2.69E-10
	8125-4	1.68E+06	2.3E+04	1.0245E+00	3.07E+00	6.99E-02	0.171	2.33E-10
7H-5, 107-109	8126-1	2.01E+06	2.1E+04	1.2260E+00	5.95E+00	4.84E-02	0.288	2.79E-10
	8126-2	2.01E+06	1.6E+04	1.2274E+00	1.75E+00	3.94E-02	0.335	2.92E-10
	8126-3	2.21E+06	1.7E+04	1.3509E+00	3.37E+00	2.03E-01	0.626	1.86E-10
	8126-4	2.00E+06	1.3E+04	1.2229E+00	3.23E+00	4.40E-02	0.477	2.86E-10
	8126-5	2.02E+06	2.3E+04	1.2314E+00	4.16E+00	2.01E-02	0.251	2.96E-10
	8126-6	2.01E+06	1.7E+04	1.2292E+00	2.38E+00	5.66E-02	0.273	2.91E-10
	8126-7	2.08E+06	4.9E+04	1.2669E+00	5.89E+00	4.44E-02	0.111	2.70E-10
	8126-8	2.09E+06	4.6E+04	1.2744E+00	6.54E+00	8.45E-01	0.214	1.23E-10
	8126-9	2.06E+06	3.1E+04	1.2579E+00	6.44E+00	3.21E-02	0.125	2.74E-10
	8126-10	2.02E+06	1.9E+04	1.2322E+00	5.41E+00	3.60E-02	0.284	2.68E-10
	8126-11	2.01E+06	8.2E+03	1.2276E+00	4.42E+00	5.42E-02	0.679	2.60E-10
	8126-12	2.02E+06	1.2E+04	1.2329E+00	2.94E+00	6.77E-02	0.431	2.83E-10
	8126-13	1.98E+06	3.8E+03	1.2114E+00	1.14E+00	4.01E-02	1.585	2.72E-10
7H-6,108-122	8079-1	2.09E+06	3.6E+04	1.2937E+00	6.67E+00	7.55E-02	0.192	2.47E-10
	8079-2	2.26E+06	3.7E+04	1.3998E+00	2.12E+01	3.68E-01	0.680	1.30E-10
	8079-3	1.99E+06	2.8E+04	1.2307E+00	1.59E+01	4.09E-02	1.242	2.69E-10
	8079-4	2.09E+06	3.4E+04	1.2928E+00	3.18E+01	9.09E-02	0.635	2.58E-10
	8079-5	2.01E+06	3.5E+04	1.2471E+00	2.79E+01	3.84E-02	0.568	2.71E-10
	8079-6	2.66E+06	6.1E+04	1.6478E+00	4.52E+01	5.01E-01	0.771	1.21E-10
	8079-7	2.04E+06	3.9E+04	1.2630E+00	3.15E+01	2.89E-02	0.253	3.05E-10
	8079-8	1.95E+06	5.6E+04	1.2079E+00	3.24E+01	2.83E-02	0.241	2.70E-10
	8079-9	2.15E+06	3.7E+04	1.3355E+00	2.02E+01	3.83E-02	0.426	2.77E-10
	8079-10	2.00E+06	4.0E+04	1.2406E+00	3.02E+01	3.52E-02	0.242	2.72E-10
	8079-11	2.03E+06	4.0E+04	1.2573E+00	2.21E+01	5.34E-02	0.320	2.83E-10

Table 3 (continued).

Core, section, interval (cm)	Lab number	Age (yr)	1σ (yr)	$^{40}Ar^*/^{39}Ar_K$	% $^{40}Ar_{atm}$	Ca/K	Mass (mg)	Volume ^{39}Ar (ccSTP/mg)
8H-3, 14-19	8080-1	2.03E+06	2.9E+04	1.2607E+00	2.80E+00	4.47E-02	0.254	2.48E-10
	8080-2	2.58E+06	4.6E+04	1.5984E+00	2.67E+01	3.95E-01	2.278	1.27E-10
	8080-3	2.12E+06	4.4E+04	1.3156E+00	3.53E+01	8.83E-02	0.824	1.86E-10
	8080-4	2.52E+06	2.7E+05	1.5632E+00	8.21E+01	1.57E+01	0.558	1.92E-11
	8080-5	2.00E+06	3.6E+04	1.2399E+00	1.86E+01	3.06E-02	0.528	2.81E-10
	8080-6	2.01E+06	4.7E+04	1.2459E+00	3.58E+01	6.10E-02	0.265	2.55E-10
	8080-7	2.19E+06	6.3E+04	1.3561E+00	2.83E+01	5.66E-01	0.293	1.12E-10
	8080-8	2.07E+06	4.2E+04	1.2804E+00	2.09E+01	4.14E-02	0.319	2.60E-10
	8080-9	2.01E+06	6.4E+04	1.2435E+00	2.99E+01	6.64E-02	0.155	2.83E-10
	8080-10	1.98E+06	4.4E+04	1.2284E+00	2.77E+01	2.87E-02	0.312	2.60E-10
	8080-11	1.97E+06	5.8E+04	1.2193E+00	4.39E+01	4.39E-02	0.267	2.35E-10
8H-6, 20-26	8081-1	2.17E+06	3.6E+04	1.3213E+00	4.33E+00	3.60E-01	0.278	1.83E-10
	8081-2	2.13E+06	4.2E+04	1.2963E+00	7.75E+00	3.37E-01	0.220	1.92E-10
	8081-3	2.13E+06	3.3E+04	1.2956E+00	1.08E+01	3.68E-01	0.315	1.88E-10
	8081-4	2.14E+06	1.1E+05	1.2991E+00	1.20E+01	4.92E-01	0.105	1.93E-10
	8081-5	2.05E+06	4.4E+04	1.2470E+00	1.09E+01	5.63E-01	0.247	1.35E-10
	8081-6	2.17E+06	4.8E+04	1.3162E+00	8.18E+00	3.89E-01	0.183	1.70E-10
9H-1, 33-34	8128-1	2.19E+06	2.6E+04	1.3349E+00	2.73E+00	7.51E-02	0.184	2.84E-10
	8128-2	2.31E+06	5.0E+04	1.4096E+00	4.01E-01	5.11E-02	0.084	3.12E-10
	8128-3	2.27E+06	4.0E+04	1.3885E+00	1.09E+00	5.25E-02	0.108	3.24E-10
	8128-4	2.27E+06	8.1E+04	1.3878E+00	2.27E+00	7.93E-02	0.056	3.13E-10
	8128-5	2.28E+06	6.4E+04	1.3899E+00	1.17E+00	6.57E-02	0.064	3.20E-10
	8128-6	2.23E+06	1.4E+05	1.3611E+00	4.56E+00	7.22E-02	0.065	1.47E-10
	8128-7	2.29E+06	4.9E+04	1.3989E+00	1.34E+00	6.14E-02	0.079	2.67E-10
9H-2, 36-42	8083-1	2.69E+06	3.3E+05	1.6342E+00	2.28E+01	1.51E+01	0.170	2.48E-11
	8083-2	2.16E+06	2.9E+04	1.3146E+00	5.66E+00	9.05E-02	0.518	2.72E-10
	8083-3	2.19E+06	3.0E+04	1.3340E+00	2.31E+00	6.27E-02	0.433	2.70E-10
	8083-4	2.14E+06	4.2E+04	1.2990E+00	4.12E+00	3.67E-02	0.167	2.62E-10
	8083-5	2.19E+06	3.9E+04	1.3337E+00	5.63E+00	1.81E-01	0.305	1.93E-10
	8083-6	2.39E+06	4.1E+04	1.4536E+00	7.70E+00	2.02E-01	0.349	1.56E-10
	8083-7	2.29E+06	4.6E+04	1.3892E+00	7.27E+00	7.35E-02	0.205	2.04E-10
	8083-8	2.18E+06	4.2E+04	1.3257E+00	3.94E+00	5.38E-02	0.148	2.63E-10
	8083-9	3.01E+06	5.9E+05	1.8320E+00	3.96E+01	3.63E+01	0.192	1.19E-11
	8083-10	1.88E+06	4.1E+05	1.1402E+00	3.87E+01	6.77E+00	0.153	3.10E-11
11H-2, 68-70	8130-1	2.43E+06	2.7E+04	1.4858E+00	7.00E+00	4.92E-02	0.150	2.40E-10
	8130-2	2.49E+06	9.1E+04	1.5225E+00	5.29E+00	5.30E-02	0.074	2.32E-10
	8130-3	2.53E+06	4.8E+04	1.5426E+00	4.33E+00	4.80E-02	0.182	2.28E-10
	8130-4	2.51E+06	7.1E+04	1.5304E+00	6.38E+00	3.88E-02	0.104	2.52E-10
	8130-5	2.57E+06	8.2E+04	1.5663E+00	1.86E+00	5.76E-02	0.097	2.35E-10
	8130-6	2.48E+06	6.6E+04	1.5135E+00	3.56E+00	6.07E-02	0.138	2.15E-10
	8130-7	2.46E+06	9.9E+04	1.5000E+00	5.54E+00	5.90E-02	0.113	2.13E-10
	8130-8	2.53E+06	5.2E+04	1.5457E+00	6.95E+00	7.03E-02	0.174	2.04E-10
	8130-9	2.59E+06	1.1E+05	1.5844E+00	6.61E+00	1.36E-01	0.068	2.26E-10
	8130-10	2.53E+06	6.0E+04	1.5429E+00	7.63E+00	5.87E-02	0.113	2.26E-10
	8130-11	2.40E+06	4.8E+04	1.4670E+00	1.06E+01	3.59E-02	0.118	2.03E-10
	8130-12	2.44E+06	6.5E+04	1.4887E+00	6.63E+00	9.19E-03	0.083	2.17E-10
	8130-13	2.41E+06	4.4E+04	1.4697E+00	8.60E+00	1.87E-02	0.095	2.19E-10

Notes: The single crystal $^{40}Ar/^{39}Ar$ ages above include analytical uncertainties, argon isotope compositions, Ca/K ratios, mass, and volume. Also included is the ^{39}Ar release of feldspar crystals from Pliocene–Pleistocene fallout tephra layers and volcaniclastic sediments from Holes 953A, 954A, 954B, and 956A.

cm. Two anorthoclase crystals give apparent ages of 13.03 ± 0.04 and 13.49 ± 0.04 Ma; two crystals are ~1.6 to 1.8 Ma, seven crystals range in age from 0.86 ± 0.01 Ma to 0.98 ± 0.01 Ma, the youngest crystal constraining the maximum age of the deposit.

Sample 157-954A-9H-4, 26–31 cm, represents a crystal lithic volcaniclastic sand with abundant small, well-rounded pumice pebbles. Eleven crystals (0.10–0.38 mg) were analyzed, comprising two anorthoclase feldspars with ages of 12.94 ± 0.04 and 9.96 ± 0.03 Ma, three with apparent ages ranging from 1.8 ± 0.1 to 2.8 ± 0.4 Ma, and six plagioclase crystals whose individual ages (0.6 ± 0.4 to 1.6 ± 0.2 Ma) are compatible with a mean apparent age of 1.15 ± 0.04 Ma (MSWD = 2.22; maximum age estimate for the deposit).

Sample 157-954B-1R-1, 64–72 cm, is from highly heterolithologic lapillistone breccia beds consisting of angular to well-rounded, aphyric phonolite, scoria and lava fragments, grey pumice, glass shards, bioclasts, and fossil shells. Only five feldspar crystals (0.15–1.29 mg) were recovered, one of which yielded an apparent age of 13.75 ± 0.05 Ma. The remaining three anorthoclase and one plagioclase crystals show isochronous argon compositions (age = 1.43 ± 0.07 Ma; initial $^{40}Ar/^{36}Ar$ ratio = 325 ± 55; MSWD = 0.22). Their mean apparent age of 1.46 ± 0.04 Ma gives a maximum age estimate for the deposition of Sample 157-954B-1R-1, 64–72 cm.

Sample 157-956A-3H-2, 81–87 cm, represents a calcareous turbidite sand layer with abundant volcanic lithics, pumice and crystals. Eleven anorthoclase crystals that were dated range in age from 0.244 ± 0.006 Ma to 0.73 ± 0.01 Ma.

Sample 157-956A-6H-1, 5–12 cm, is a coarse volcaniclastic sand deposit with basalt and pumice pebbles. Eleven anorthoclase crystals were separated from the ash fraction and show apparent ages from 1.42 ± 0.15 to 1.76 ± 0.09 Ma. Isotope correlation gives an isochron with an age of 1.71 ± 0.04 Ma (initial = 260 ± 110; MSWD = 0.54), largely overlapping with the mean apparent age of 1.68 ± 0.02 Ma (MSWD = 0.78) within error limits.

Sample 157-956A-6H-2, 120–122 cm, represents well-sorted, pumice-bearing volcaniclastic sand deposits. Two anorthoclase crystals were dated and give a mean apparent age of 1.67 ± 0.02 Ma.

Sample 157-956A-6H-2, 124–126 cm, is a volcaniclastic pumice sand. Four feldspar crystals were dated and give an isochron age of 1.71 ± 0.02 Ma (initial = 260 ± 110; MSWD = 0.54), and a mean apparent age of 1.70 ± 0.01 Ma (MSWD = 0.39).

Sample 157-956A-7H-5, 107–109 cm, represents the top of an 8-cm thin crystal- and pumice-rich volcaniclastic sand. Thirteen crystals were dated, 12 of which yield an isochron (age = 1.98 ± 0.07 Ma; initial = 437 ± 38; MSWD = 0.38), and an error-weighted average age of 2.00 ± 0.05 Ma (MSWD = 2.89). One crystal is significantly older (2.21 ± 0.02 Ma).

Sample 157-956A-7H-6, 108–122 cm, is a poorly sorted, crystal-rich volcaniclastic sand with abundant well-rounded pumice pebbles.

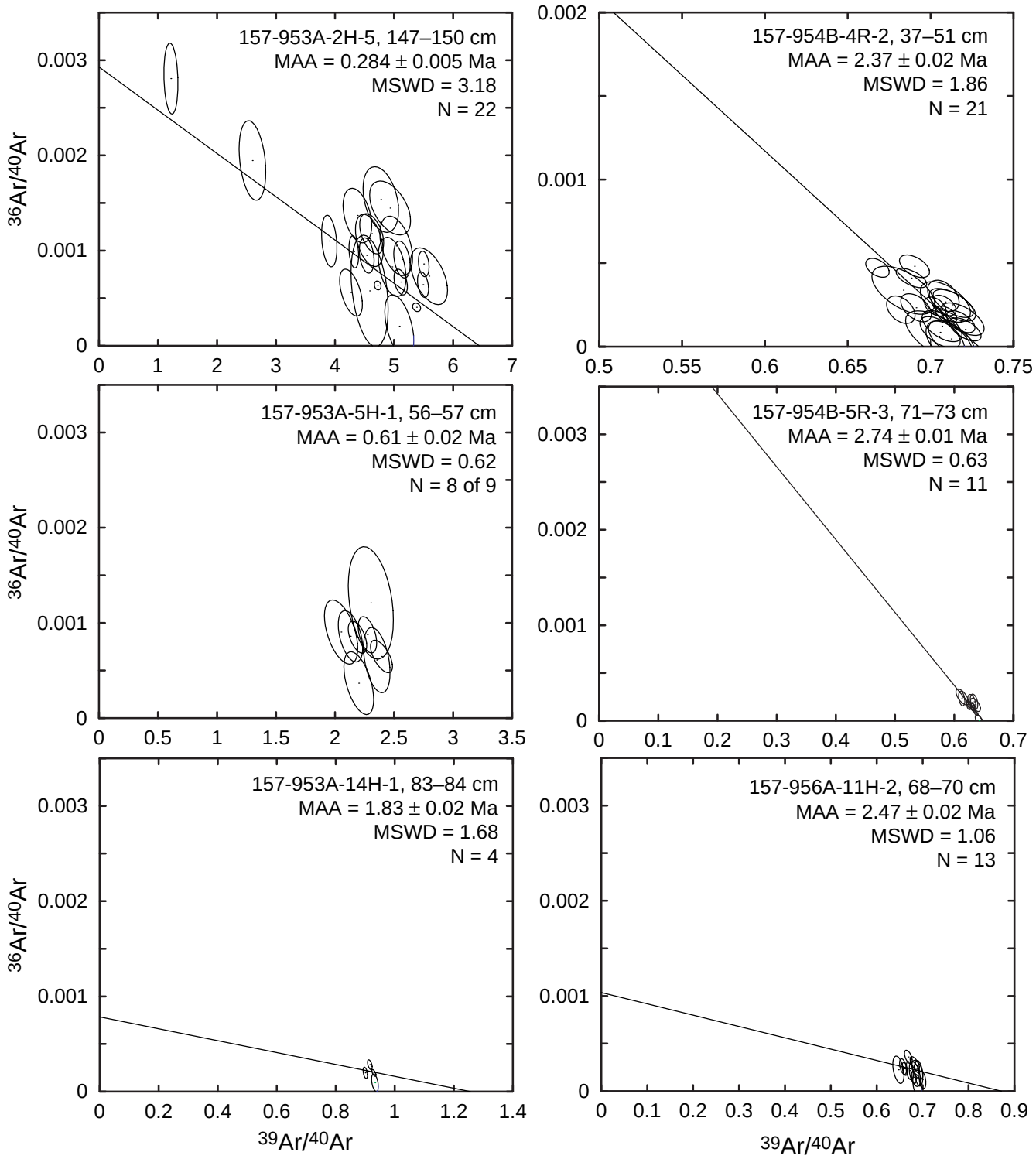

Figure 2. Isotope correlation diagrams showing the argon isotope composition of feldspar crystals from fallout tephra layers in Holes 953A, 954B, and 956A. MAA = Mean apparent ages, weighted by the inverse of the variance. Numerical results of the isochrons are given in Table 2. Crystals from Sample 157-953A-5H-1, 56-57 cm, yield fit with negative initial. All analyses are normalized to a common J-value of 1E-3.

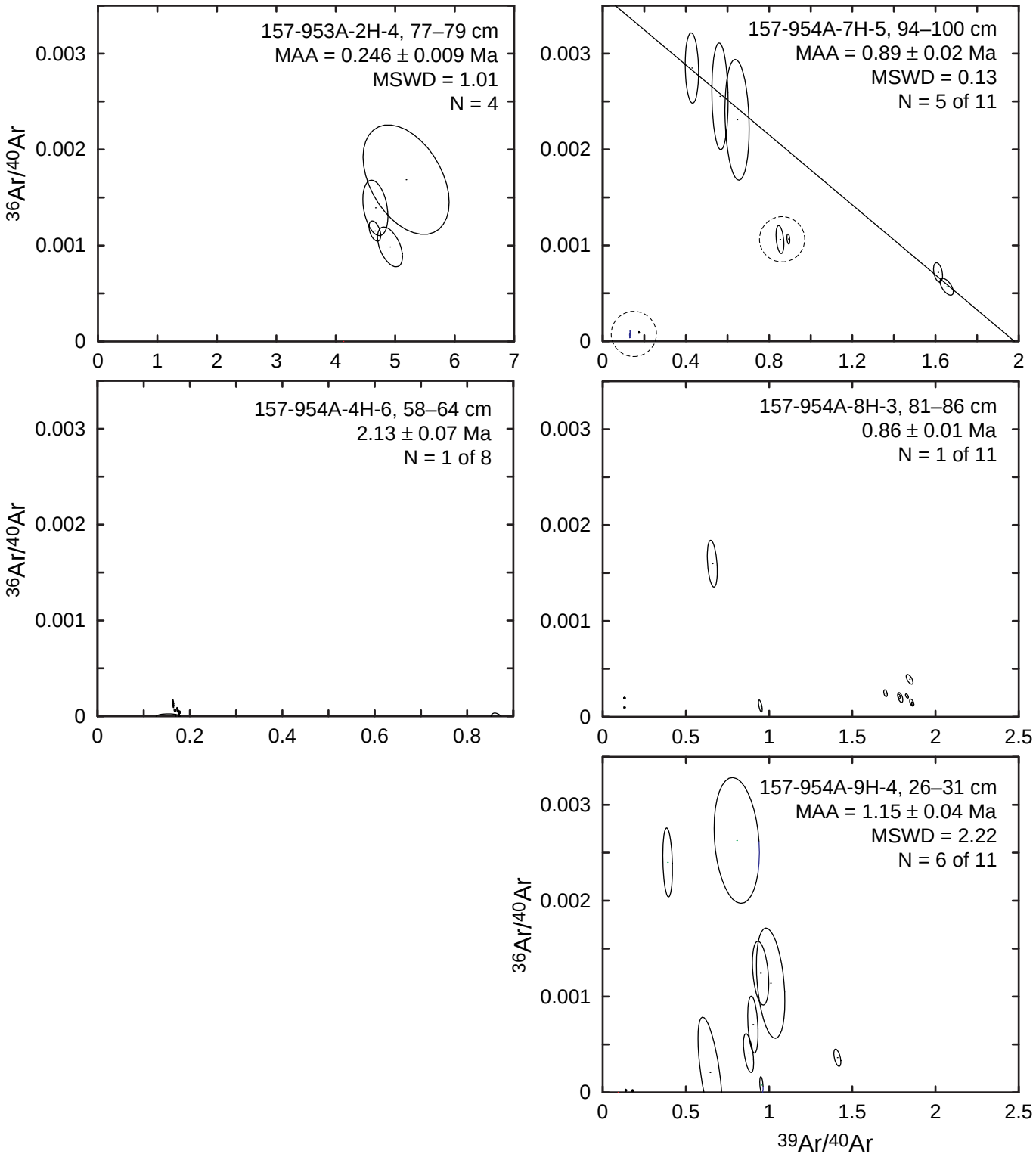

Figure 3. Isotope correlation diagrams showing the argon isotope composition of feldspar crystals from volcaniclastic deposits in Holes 953A, 954A, 954B, and 956A. MAA = Mean apparent ages, weighted by the inverse of the variance. Numerical results of the isochrons are given in Table 2. Encircled data points have been excluded from the isochron and mean apparent age calculations. No meaningful isochrons have been obtained for Samples 157-953A-2H-4, 77–79 cm; 157-954A-4H-6, 58–64 cm; 8H-3, 81–86 cm; 9H-4, 26–31 cm; 157-956A-3H-2, 81–87 cm; 157-956A-9H-1, 33–34 cm; and 9H-2, 36–42 cm, because of fits with negative initial $^{40}Ar/^{36}Ar$ ratios and/or highly heterogeneous age populations. All analyses are normalized to a common J-value of 1E-3.

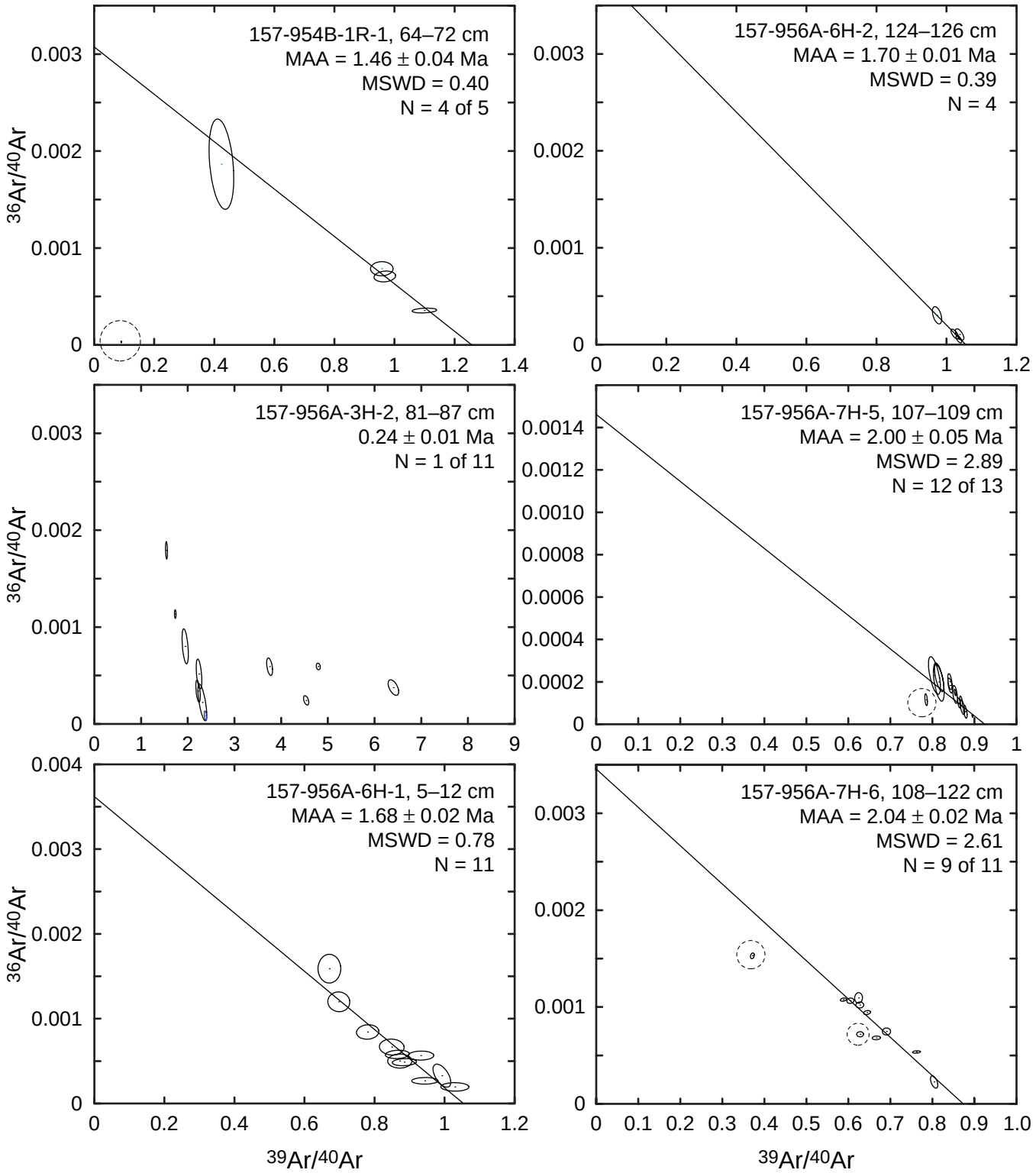

Figure 3 (continued).

Eleven crystals were dated, nine giving an isochron (age = 2.06 ± 0.06 Ma; initial $^{40}Ar/^{36}Ar$ ratio = 289 ± 26; MSWD = 3.04), and an error-weighted average age of 2.04 ± 0.02 Ma (MSWD = 2.61). Two crystals are significantly older (2.26 ± 0.04 Ma and 2.66 ± 0.06 Ma).

Sample 157-956A-8H-3, 14–19 cm, represents a poorly sorted, massive volcaniclastic sand with nannofossil clay matrix, dominated by basaltic lithic clasts and rounded pumice clasts. Eleven crystals were dated, 10 defining an isochron (age = 2.03 ± 0.03 Ma; initial $^{40}Ar/^{36}Ar$ ratio = 303 ± 8; MSWD = 1.83), and an error-weighted average age of 2.04 ± 0.02 Ma (MSWD = 1.99). One crystal is significantly older (2.58 ± 0.05 Ma).

Sample 157-956A-8H-6, 20–26 cm, is from a fine-grained, massive but normally graded, calcareous, pumiceous volcaniclastic silt. All six anorthoclase crystals dated yield ages from 2.13 ± 0.03 Ma to

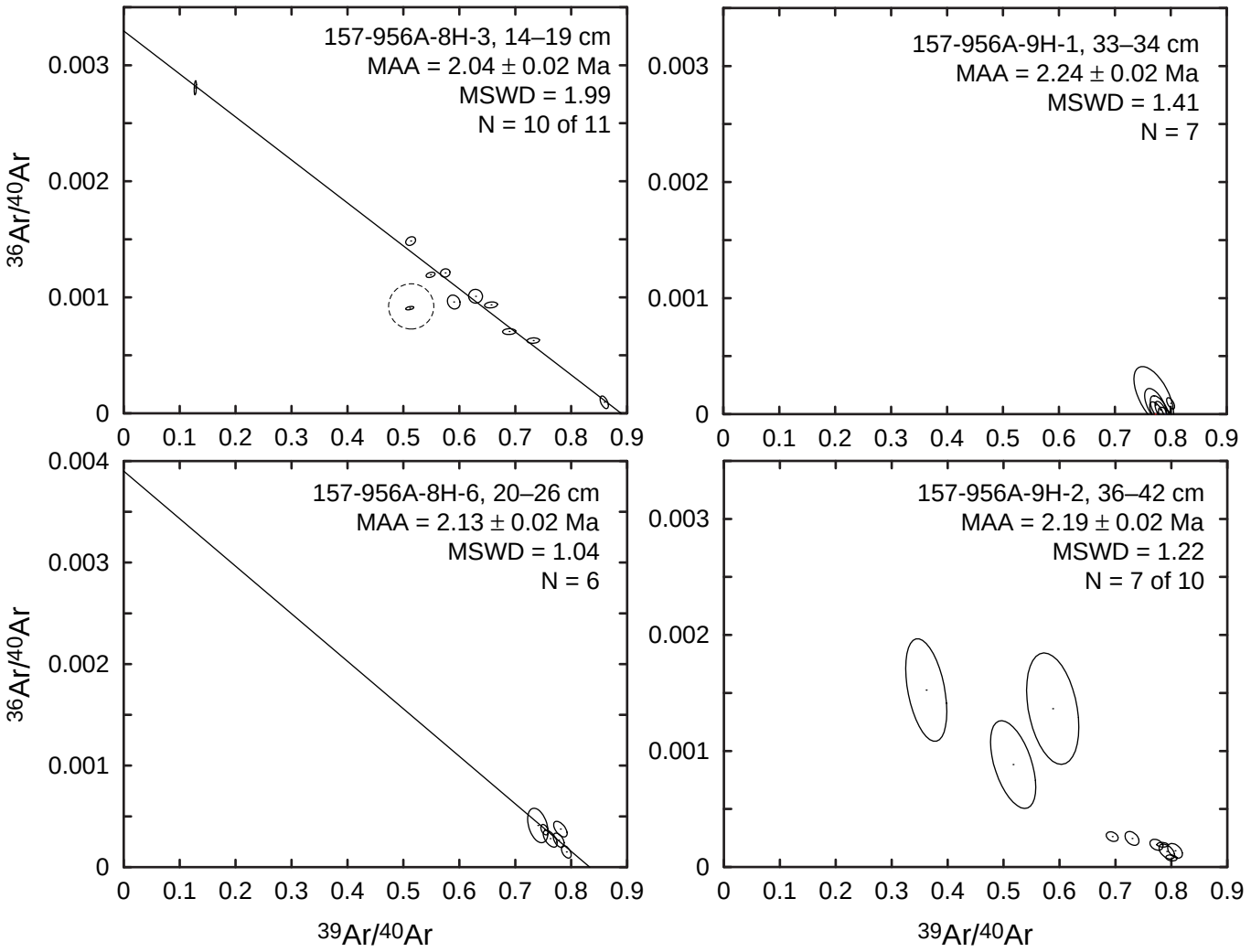

Figure 3 (continued).

2.17 ± 0.04 Ma, and an isochron age of 2.16 ± 0.04 Ma (initial $^{40}Ar/^{36}Ar$ ratio = 256 ± 204; MSWD = 1.31), their mean apparent age being 2.13 ± 0.02 Ma (MSWD = 1.04).

Sample 157-956A-9H-1, 33–34 cm, represents a well-sorted foraminifer volcaniclastic sand rich in volcanic glass shards and crystals. All seven anorthoclase crystals dated yield ages from 2.19 ± 0.03 Ma to 2.31 ± 0.05 Ma, an isochron with a negative initial, but a mean apparent age of 2.24 ± 0.02 Ma (MSWD = 1.41).

Sample 157-956A-9H-2, 36–42 cm, is from the basal, inversely graded section of a 39-cm-thick, pumiceous volcaniclastic sand. Ten crystals were dated. Three plagioclase crystals give apparent ages from 1.9 ± 0.4 Ma to 3.0 ± 0.6 Ma. The ages of seven anorthoclase feldspars range from 2.14 ± 0.04 Ma to 2.39 ± 0.04 Ma. Only seven of the 10 crystals (6 K-feldspar + 1 plagioclase) yield concordant ages, and a mean apparent age of 2.19 ± 0.02 Ma (MSWD = 1.22) as maximum age estimate for this deposit.

CONCLUSIONS

Fallout tephra layers from the upper 100 to 120 mbsf at Holes 953A, 954A, 954B, and 956A erupted between 0.28 Ma and 2.74 Ma. The ash beds show isotopically homogeneous crystal populations and form chronostratigraphic markers at 15.08 mbsf (0.273 ± 0.006 Ma); 36.66 mbsf (0.61 ± 0.02 Ma); 122.43 mbsf (1.83 ± 0.02 Ma) in lithologic Unit I of Hole 953A (Fig. 4); at 111.61 mbsf (2.37 ± 0.02 Ma); 123.01 mbsf (2.74 ± 0.01 Ma) in lithologic Unit I of Hole 954A and 954B (Fig. 5); and 93.78 mbsf (2.47 ± 0.02 Ma) in lithologic Subunit IC of Hole 956A (Fig. 6). In the 0 to ~2 Ma stratigraphic interval, the $^{40}Ar/^{39}Ar$ ages of the fallout ash layers are perfectly compatible with the age and sedimentation rate estimates from nannofossil and paleomagnetic chronostratigraphies (Fig. 4). Three ash layers with eruption ages from 2.3 to 2.7 Ma, however, either fall at the minimum age boundaries or are even significantly younger (157-956A-11H-2, 68–70 cm) than the stratigraphic ages derived from nannofossil and paleomagnetic time scales (Figs. 5, 6).

During the last 3 k.y., explosive volcanism in the Canaries archipelago was governed by eruptions of basaltic magmas on La Palma and Gran Canaria (Post Roque Nublo Formation), and frequent eruptions of basaltic and highly differentiated peralkaline magmas on Tenerife. Considering the petrologic evolution and radiometric ages of explosive eruptions from the potential ocean island sources (Schmincke, 1976; Lietz and Schmincke, 1975; McDougall and Schmincke, 1977; Ancochea et al., 1990; Marti et al., 1994; Bogaard and Schmincke, Chap. 11, this volume), and the mineral composition and $^{40}Ar/^{39}Ar$ ages of the Pliocene–Pleistocene fallout tephra layers in Holes 953A, 954A, 954B, and 956A, the fallout tephra layers are interpreted to be derived from explosive eruption of the Cañadas

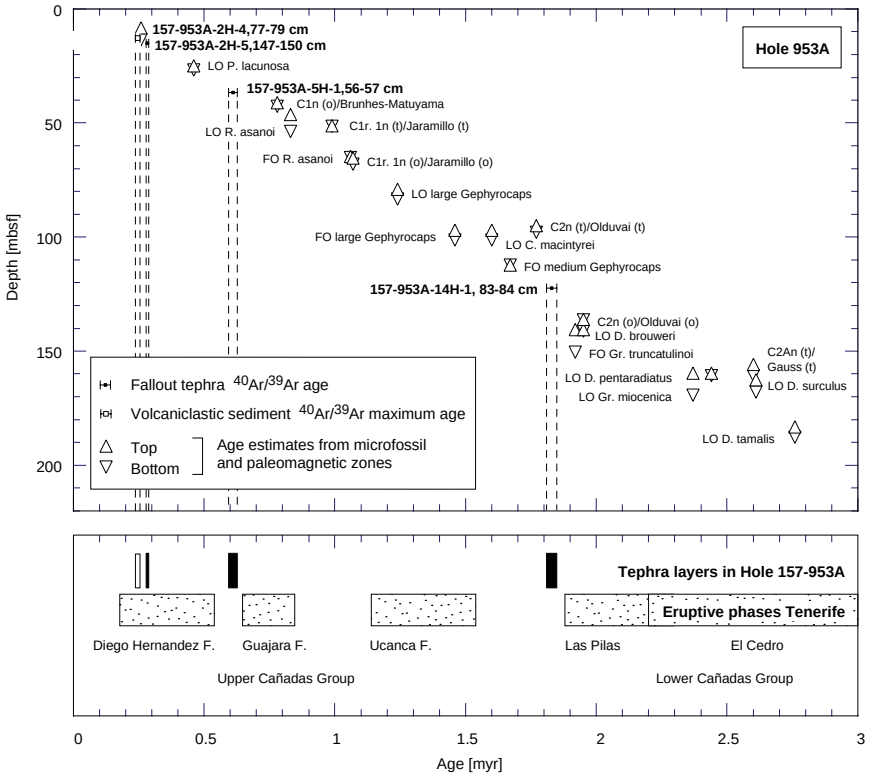

Figure 4. **Top.** Depth-age diagram showing the ^{40}Ar/^{39}Ar ages of fallout tephra layers and ^{40}Ar/^{39}Ar maximum sedimentation ages of volcaniclastic deposits from Hole 953A compared to age points derived from nannofossil and paleomagnetic chronostratigraphies. **Bottom.** Ages of fallout tephra layers (solid boxes) and volcaniclastic deposits (open boxes) compared to the land-based chronology of explosive eruptions from Cañadas Caldera, Tenerife (Marti et al., 1994). Box widths indicate 1 sigma error limits of dates. Nannofossil data and paleomagnetic reversals from Schmincke, Weaver, Firth, et al. (1995).

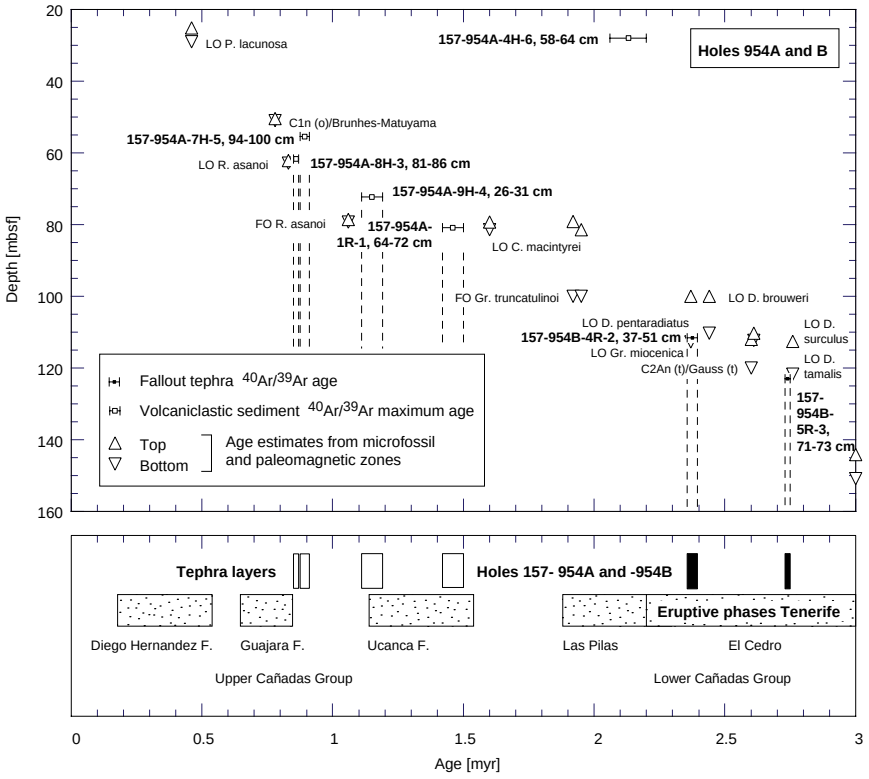

Figure 5. **Top.** Depth-age diagram showing the ^{40}Ar/^{39}Ar ages of fallout tephra layers and ^{40}Ar/^{39}Ar maximum sedimentation ages of volcaniclastic deposits from Holes 954A and 954B compared to age points derived from nannofossil and paleomagnetic chronostratigraphies. **Bottom.** Ages of fallout tephra layers (solid boxes) and volcaniclastic deposits (open boxes) compared to the land-based chronology of explosive eruptions from Cañadas Caldera, Tenerife (Marti et al., 1994). Box widths indicate 1 sigma error limits of dates. Nannofossil data and paleomagnetic reversals from Schmincke, Weaver, Firth, et al. (1995).

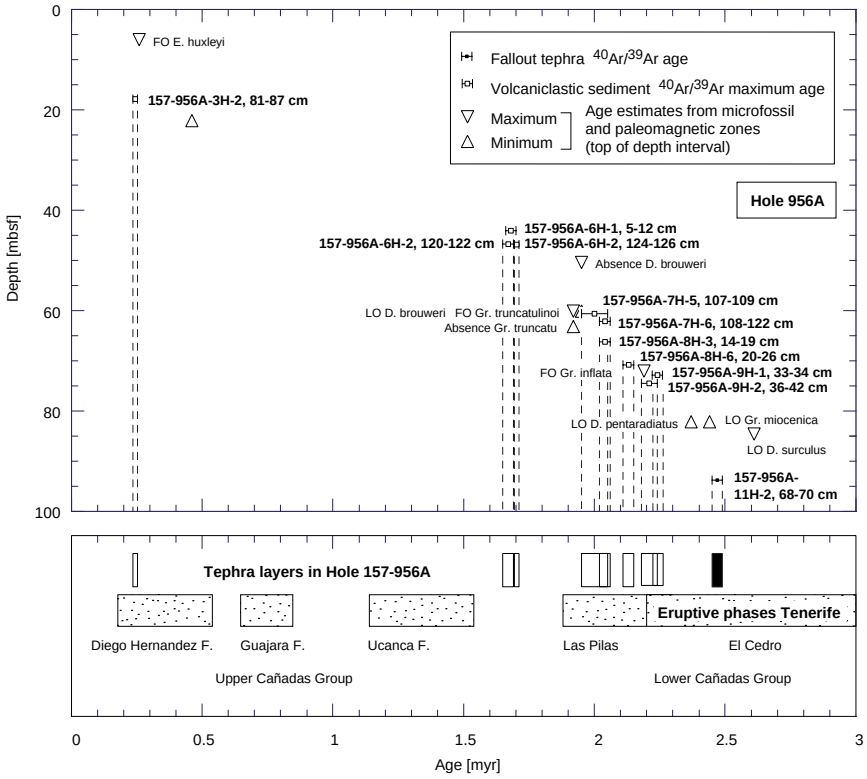

Figure 6. **Top.** Depth-age diagram showing the $^{40}Ar/^{39}Ar$ ages of fallout tephra layers and $^{40}Ar/^{39}Ar$ maximum sedimentation ages of volcaniclastic deposits from Hole 956A compared to age points derived from nannofossil chronostratigraphy. **Bottom.** Ages of fallout tephra layers (solid boxes) and volcaniclastic deposits (open boxes) compared to the land-based chronology of explosive eruptions from Cañadas Caldera, Tenerife (Marti et al., 1994). Box widths indicate 1 sigma error limits of dates. Nannofossil data from Schmincke, Weaver, Firth, et al. (1995).

Caldera, Tenerife. The two younger fallout ash beds dated from Hole 953A (Sample 157-953-2H-5, 147–150 cm, and 5H-1, 56–57 cm) can be correlated with the eruptive interval of the Upper Cañadas Group, whereas those from Core 157-953A-14H and Holes 954A, 954B, and 956A can be correlated with the eruptive intervals of the Las Pilas (Sample 157-953A-14H-1, 83–84 cm) and El Cedro Formations (Sample 157-954B-4R-2, 37–51 cm; 5R-3, 71–73 cm; and Sample 157-956A-11H-2, 68–70 cm) of the Lower Cañadas Group of Marti et al. (1994; Figs. 4–6).

As indicated by their $^{40}Ar/^{39}Ar$ maximum ages and single crystal age spectra, all volcaniclastic layers from the 0 to 3 Ma interval of Holes 953A, 954A, 954B, and 956A represent tephra material from explosive eruptions of the Cañadas Caldera of Tenerife too, which was mixed with older sediment material and crystals during reworking. The single crystal age spectra, however, show a striking difference between the Pliocene–Pleistocene volcaniclastic deposits north (Holes 954A and 954B) and southwest (Hole 956A) of Gran Canaria (Fig. 7). Older feldspar crystals, derived from Miocene volcanics, are only present in the northern cores: five of seven volcaniclastic ash beds from Holes 954A and 954B contain crystals from reworked deposits of the Middle Mogán to Upper Fataga eruptive phases of Gran Canaria. Volcaniclastic deposits from the southwestern site, in contrast, exclusively contain crystals from Pliocene–Pleistocene (Tenerife-derived) volcanic sediments. Surprisingly, sediment material from the Roque Nublo Formation of Gran Canaria (which comprises several major eruptions of phonolitic, feldspar-phyric magmas) and from the Anaga to Roque del Conde Formations of Tenerife, which immediately precede the Cañadas eruptive phase, appear to be lacking or subordinate in the Pliocene–Pleistocene volcaniclastic sediments studied.

The $^{40}Ar/^{39}Ar$ ages of fallout tephra and volcaniclastic ash layers from Sites 953, 954, and 956 also cast new light on the eruption record of the Cañadas magma system. Based on a detailed survey and K-Ar and $^{40}Ar/^{39}Ar$ age determinations of near-vent tephra sequences exposed in the Cañadas Caldera wall, Marti et al. (1994) concluded that the Pliocene–Pleistocene eruptive activity pattern of Tenerife is governed by discrete cycles of activity lasting ~100 to 300 ka (Diego Hernandez, Guajara, Ucanca, Las Pilas, El Cedro Formations), which were separated by periods of dormancy of about equal duration. The $^{40}Ar/^{39}Ar$ ages of marine tephra layers 157-953A-5H-1, 56–57 cm, and 14H-1, 83–84 cm, and five of the volcaniclastic deposits of Holes 954A and 956A, however, indicate that the explosive eruptive activity of the Cañadas Caldera of Tenerife has been much more continuous during the past 3 Ma. These fallout tephra layers and volcaniclastic deposits represent eruptions that basically fill the gaps between the Diego Hernandez and Guajara Formations, and Ucanca and Las Pilas Formations (Figs. 4–6). With the possible exception of a Guajara-Ucanca break, the postulated extended periods of dormancy appear to reflect chiefly the incomplete preservation of the ocean island's explosive eruption record on land.

Apart from Sample 157-954A-4H-6, 58–64 cm, the maximum eruption age estimates obtained from the volcaniclastic sediments are in excellent agreement with the stratigraphic ages and sedimentation rates obtained from nannofossil and paleomagnetic chronostratigraphies and the eruption ages of the fallout tephra layers dated here. This shows that precise and close approximation of the actual age of deposition can be obtained directly from single crystal $^{40}Ar/^{39}Ar$ dating of the mineral components of volcaniclastic sediments.

ACKNOWLEDGMENTS

I am indebted to Uta Rodehorst for feldspar separations on several samples used in this study and Reinhard Werner for comments and suggestions on the manuscript. This research was supported by a grant from the Deutsche Forschungsgemeinschaft (Grant No. BO 912/4-1).

REFERENCES

Ancochea, E., Fúster, J.M., Ibarrola, E., Cendrero, A., Coello, J., Hernán, F., Cantagrel, J.M., and Jamond, C., 1990. Volcanic evolution of the island

of Tenerife (Canary Islands) in the light of new K-Ar data. *J. Volcanol. Geotherm. Res.*, 44:231–249.

Bogaard, P., Schmincke, H.-U., Freundt, A., Hall, C., and York, D., 1988. Eruption ages and magma supply rates during the Miocene evolution of Gran Canaria: single crystal $^{40}Ar/^{39}Ar$ laser ages. *Naturwissenschaften*, 75:616–617.

Dalrymple, G.B., and Duffield, W.A., 1988. High precision $^{40}Ar/^{39}Ar$ dating of Oligocene tephra from the Mogollon-Datil volcanic field using a continuous laser system. *Geophys. Res. Lett.*, 15:463–466.

Duffield, W.A., and Dalrymple, G.B., 1990. The Taylor Creek Rhyolite of New Mexico: a rapidly emplaced field of lava domes and flows. *Bull. Volcanol.*, 52:475–487.

Lietz, J., and Schmincke, H.-U., 1975. Miocene-Pliocene sea-level changes and volcanic phases on Gran Canaria (Canary Islands) in the light of new K-Ar ages. *Palaeogeogr., Palaeoclimatol., Palaeoecol.*, 18:213–239.

Marti, J., Mitjavila, J., and Araña, V., 1994. Stratigraphy, structure, age and origin of the Cañadas Caldera (Tenerife, Canary Islands). *Geol. Mag.*, 131:715–727.

McDougall, I., and Schmincke, H.-U., 1977. Geochronology of Gran Canaria, Canary Islands: age of shield-building volcanism and other magmatic phases. *Bull. Volcanol.*, 40:1–21.

Schmincke, H.-U., 1976. The geology of the Canary Islands. *In* Kunkel, G. (Ed.), *Biogeography and Ecology in the Canary Islands:* The Hague (W. Junk), 67–184.

Schmincke, H.-U., and Bogaard, P.V.D., 1990. Tephra layers and tephra events. *In* Einsele, G., Ricken, W., and Seilacher, A. (Eds.), *Cycles and Events in Stratigraphy:* Berlin (Springer-Verlag), 392–429.

Schmincke, H.-U., Weaver, P.P.E., Firth, J.V., et al., 1995. *Proc. ODP, Init. Repts.*, 157: College Station, TX (Ocean Drilling Program).

York, D., 1969. Least-squares fitting of a straight line with correlated errors. *Earth Planet. Sci. Lett.*, 5:320–324.

Date of initial receipt: 3 July 1996
Date of acceptance: 26 November 1996
Ms 157SR-141

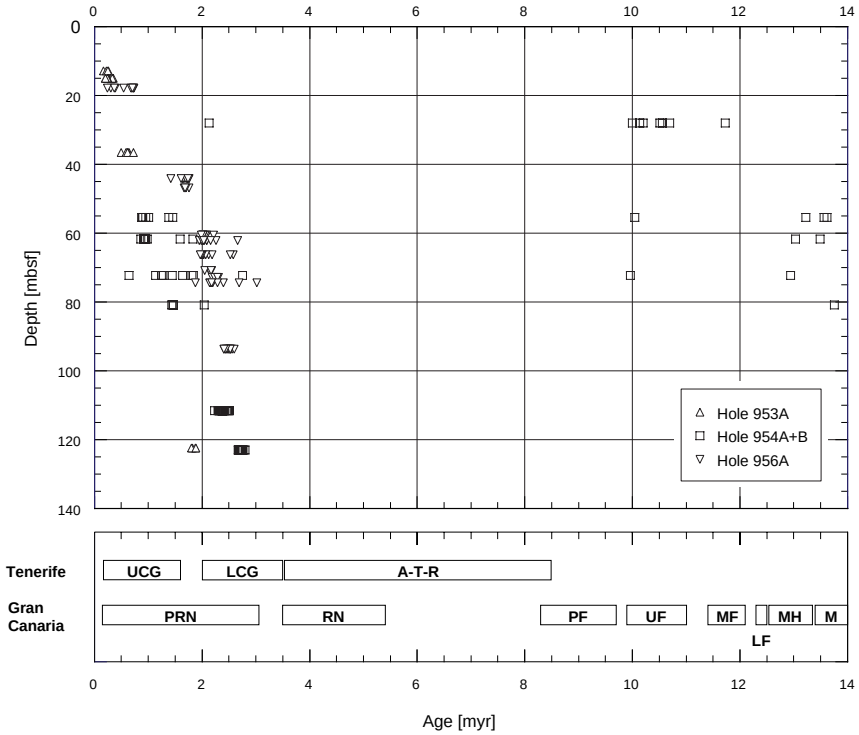

Figure 7. Depth-age diagram showing the range of single crystal ages obtained for fallout tephra layers and volcaniclastic sediments from Holes 953A, 954A, 954B, and 956A compared to the Miocene to Pleistocene eruptive phases of Gran Canaria and Tenerife. Gran Canaria: M = Mogán Group; MH = Montaña Horno Formation; LF, MF, and UF = Lower, Middle, and Upper Fataga Formations; LF = Las Palmas Formation; RN = Roque Nublo Group; PRN = Post Roque Nublo Group (based on Lietz and Schmincke, 1975; Mcdougall and Schmincke, 1977; Bogaard et al., 1988; Bogaard and Schmincke, Chap. 11, this volume). Tenerife: UCG and LCG = Upper and Lower Cañadas Group, A-T-R = Anaga, Teno, and Roque del Conde (based on Ancochea et al., 1990; Marti et al., 1994).